Materials Science-Poland, 39(4), 2021, pp. 626-638
http://www.materialsscience.pwr.wroc.pl/
DOI: 10.2478/msp-2022-0003

sciendo

Physico-mechanical properties, structure, and phase composition of (BeO + TiO_2)-ceramics containing TiO_2 nanoparticles (0.1–2.0 wt.%)

Alexandr Pavlov[1], Zhuldyz Sagdoldina[1], Askar Kassymov[2], Ainur Seitkanova[3], Bauyrzhan Rakhadilov[1,3], Aidar Kengesbekov[4,*]

[1]Sarsen Amanzholov East Kazakhstan University, Ust-Kamenogorsk, Kazakhstan
[2]Shakarim State University, Semey, Kazakhstan
[3]Pavlodar Pedagogical University, Pavlodar, Kazakhstan
[4]Institute of composite materials, Ust-Kamenogorsk, Kazakhstan

This research studies the effects of addition of micro- and nanoparticles of TiO_2 and variations in the firing temperature on the physico-mechanical properties of oxide-beryllium ceramics, shows the evolution of the microstructure of such ceramics during sintering, and presents the data of X-ray phase analysis. It was shown that the addition of TiO_2 nanoparticles leads to a higher density of the ceramic material after sintering due to the interpenetration of TiO_2 and BeO phases, which is caused by an increase in the diffusion mobility of atoms that can in turn be attributed to an increase in the imperfection of the structure and the fraction of grain boundaries. It was found that the presence of nanoparticles contributes to an increase in the apparent density of the material, as well as a decrease in its total and closed porosity; and an increase in the sintering temperature contributes to the transformation of the crystalline structure of TiO_2 into a more conductive $Ti_3O_5$with an orthorhombic structure. The presence of nanoparticles also promotes self-healing of micropores, which can be explained by the blocking of a certain fraction of the interfaces between BeO particles by nanoparticles and the creation of a diffusion barrier.

Keywords: *TiO_2 nanoparticles, beryllium oxide, titanium dioxide, ceramics, microstructure, physico-mechanical properties*

1. Introduction

Recently, much attention has been paid to research into the synthesis of nanophase high-temperature ceramics. The unique properties of nanocomposites, such as low weight, high mechanical strength, thermal conductivity, increased density, and excellent electronic properties, motivate researchers to explore their fundamental properties and develop their practical applications [1]. Of particular interest are the studies of the dielectric properties of ceramics whose frequency of absorbing mircrowave radiation is in the range of 8.2–12.4 GHz (range x) [2]. This effect is due to unique structural and electrophysical properties. A significant step forward in developing absorbers for powerful electro-vacuum devices was creating an absorbing material of the semiconductor-dielectric type with specified large values of dielectric losses and electrical conductivity in the low-frequency range characteristic of structurally inhomogeneous materials [3]. Such materials are called bulk absorbers of microwave energy, and they are obtained based on oxides [4]. Titanium in the form of TiO_2 was chosen as an ion capable of changing the valence and satisfying a set of requirements necessary for the synthesis of materials with certain technological properties [5]. The addition of TiO_2 improves the thermal stability, dielectric losses, and dielectric permittivity of oxide ceramics [6]. Ceramic samples with nano-additives can be formed using an organic connection followed by sintering [7]. The main microwave energy absorbing phase in titanate ceramics is the compound semiconductor Ti_3O_5, which is formed during the recovery of TiO_2 oxide during fabrication, in the process of fir-

* E-mail: aidar.94.01@mail.ru

© 2021. This is an open access article distributed under the Creative Commons Attribution-NonCommercial-NoDerivatives 4.0 License.
(http://creativecommons.org/licenses/by-nc-nd/4.0/)

ing the ceramics in hydrogen. This material practically does not contain a glass phase, and the closed residual porosity does not exceed 5% [8].

Interest in composite ceramics based on beryllium oxide with introduced additives is caused by the needs of new areas of special instrument making in the development of modern systems for long-distance communication, radar and navigation, and broadband systems for special purposes [9]. The main difficulty in creating devices of this type is the combination of physical and technical factors [10]. Also, at present, the task of designing and creating an industrial technology for the production of improved W-band devices continues to be relevant [11].

It is known that the addition of TiO_2 additives into BeO ceramics after heat treatment in a reducing atmosphere is accompanied by a significant increase in electrical conductivity and the ability to absorb electromagnetic radiation in a wide frequency range [12]. Until now, the mechanism of this influence has not been fully established [13]. At present, BT-30 ceramics, with BeO + 30 wt.% TiO_2, constitute the most effective material for these purposes, although the electrical properties of this ceramic can be improved [14]. In this research, it was shown that different ratios of TiO_2, particle size, and the degree of reduction make it possible to regulate the electromagnetic absorption of such ceramics [15], and to improve its physico-mechanical properties and thereby operational characteristics [16]. Further optimization of the functional characteristics of BeO ceramics and the expansion of their application to various fields of modern technology are possible because this material lends itself to modification by the use of various additives [17], which are capable of creating various surface microstructures at the boundaries of BeO microcrystallites and pores [18]. The presence of developed interfaces and intergranular interactions, as well as a number of other factors, can affect significantly the operational characteristics of the finished product [19]. TiO_2 nanoparticles are also known to have ferromagnetic properties, which have been documented in the literature [20].

Thus, the main goal of the work was to establish the mechanisms of structure formation in BeO ceramics resultant to the addition of micro- and nanocrystalline TiO2 powders, and to determine the modus operandi by which this addition can be controlled so as to form structures with the desired parametric characteristics and properties.There is a lack of studies of the effect of TiO_2 nanoparticles on the properties of oxide-beryllium ceramics, which is associated with the uniqueness of beryllium production, in that working with BeO powders requires specialized equipment and special safety conditions, and thus these factors make it difficult, if not impossible, for scientific organizations to carry out the present study.

2. Experimental

Samples were obtained by slip casting at Keramika plant (Ust-Kamenogorsk, Republic of Kazakhstan). Highly sintered beryllium oxide powder was obtained by grinding sintered ceramic powder in vibrating mills. Table 1 shows the main characteristics of the used BeO powder.

The particle shape and the surface morphology of crystals of highly burnt BeO are shown in

Table 1. The main characteristics of the used BeO powder grade “B2”

Characteristic, batch number		b 67
Bulk density, $\rho_o \times 10^3$ kg/m^3		0.77
Specific surface S, cm^2/g		11,000
Moisture, wt.%		0.08
Element-by-element impurities content, wt.%	Boron	1.7×10^{-5}
	Silicon	7.3×10^{-3}
	Manganese	8.2×10^{-4}
	Ferrum	5.1×10^{-2}
	Magnesium	5.2×10^{-3}
	Chromium	1.0×10^{-2}
	Nickel	1.1×10^{-2}
	Aluminum	3.2×10^{-2}
	Copper	8.0×10^{-4}
	Zinc	7.5×10^{-3}
	Calcium	4.2×10^{-3}
	Silver	1.1×10^{-5}
	Cadmium	1.2×10^{-5}
	Lithium	6.7×10^{-4}
	Natrium	8.7×10^{-3}
Amount of impurities, wt.%		0.14

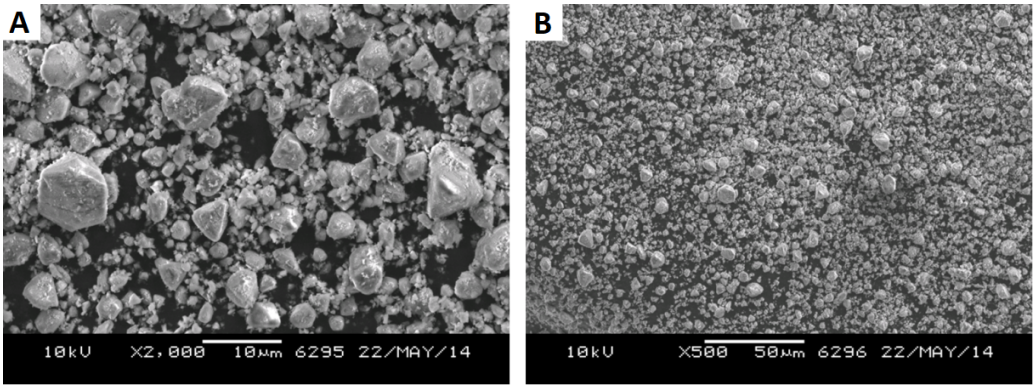


Fig. 1. Micrographs of beryllium oxide powder crystals, with a specific surface of 11,000 cm^2/g. **(A)** 2,000× magnification; **(B)** 500× magnification

Table 2. Main characteristics of the TiO_2 micron powder used

No.	**Name of indicators**	**Indicator value**	
		TC requirements, %	**Analysis results**
1	Mass fraction of titanium dioxide, %, no less	99	99.5
2	Mass fraction of rutile form, %, no less	97	100
3	Mass fraction of iron compounds in terms of Fe_2O_3, %, no more	0.08	0.05
4	Mass fraction of phosphorus compounds in terms of P_2O_5, %, no more	0.03	0.03
5	Mass fraction of sulfur compounds in terms of SiO_3, %, no more	0.03	0.01
6	Mass fraction for silicon compounds in terms of SiO_2, %, no more	0.15	0.15
7	Mass fraction of "metallic iron", %, no more	0.02	0.01
8	Specific surface, cm^2/g, within	3,300–4,600	4,060

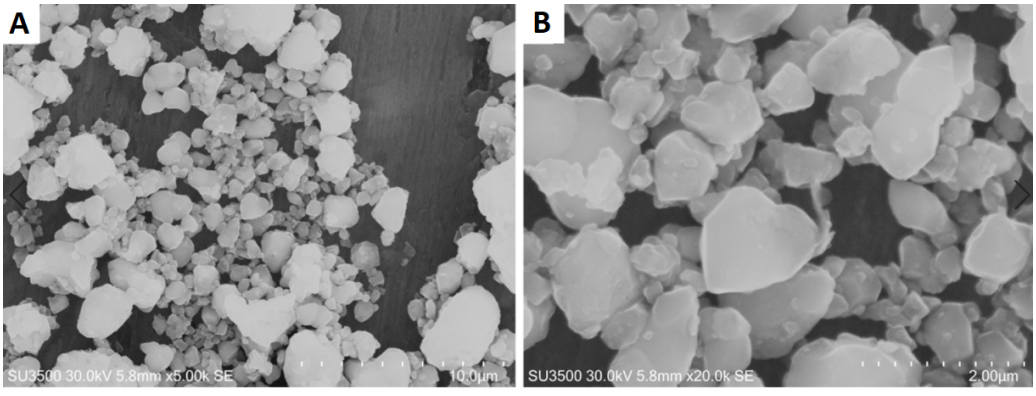


Fig. 2. Micrographs of micron titanium dioxide powders. **(A)** 5× magnification; **(B)** 20× magnification

Figure 1.

The size of the bigger crystals reaches 10 µm, and the shape of all crystals is close to spherical.

The main characteristics of the micron TiO_2 powder used in this work, which has a rutile modification in terms of quality and chemical composition according to the passport data, are given in Table 2.

Micron titanium dioxide powder was additionally sieved using a vibratory sieve through a metal mesh (No. 0045). Powders with a specific surface of at least 4,500 cm^2/g were selected. The average

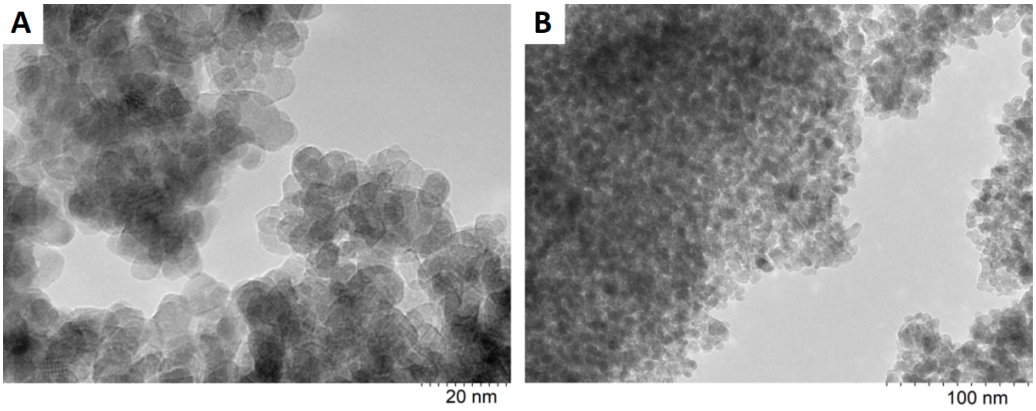


Fig. 3. Micrograph of TiO_2 nanoparticles obtained through the electric explosion of a conductor. **(A)** 400× magnification; **(B)** 100× magnification

particle size was 5–10 μm. The surface morphology and granulometric composition of the micron TiO_2 powder after sieving are shown in Figures 2A and 2B.

The TiO_2 nanopowder used in this work was obtained at the facility to synthesize nanoparticles and nanopowders by the electric explosion of a conductor.

Figures 3A and 3B show a typical micrograph of TiO_2 nanoparticles obtained through the electric explosion of a conductor. Nanopowder is a mixture of predominantly spherically shaped particles having a size of 5–10 nm.

Along with nanoparticles $\geq$ 10 nm, there are formations of agglomerates of smaller particles, and these extend up to 15 nm in size. The shape of all particles, as a rule, is close to spherical.

Slip masses containing TiO_2 nanoparticles for each batch were prepared based on an organic binder (comprised of wax, paraffin, and oleic acid) at the calculation of loss on ignition (LOI) = 14.5 wt.%. The composition of the components of the organic slip were as follows: paraffin – 82 wt.%., wax – 15 wt.%., oleic acid – 3 wt.%.

The billets were molded on a factory-made thermoplastic slip long-length casting unit.

Annealing of the organic binder (sublimation) was performed in a bogie-hearth muffle furnace in a graphite backfill (graphite grits 0.5–1.0 mm) according to a special mode for 93 h, and holding was carried out at a maximum temperature of 1,200°C for 10 h. The resulting blanks were sintered in a forevacuum in a furnace with a carbon heater, followed by reduction in a hydrogen atmosphere according to the mode: T = 800°C; the duration of the process was 1.0–1.5 h, the hydrogen consumption was 1,200 $\pm$ 50 L/h, and the pressure was 294–490 Pa.

The microstructure, particle size distribution, and phase analysis of the sintered samples were studied using a scanning electron microscope with a JSM-6390LV (JEOL, Tokyo, Japan) energy dispersive microanalysis attachment, 2007, with a resolution of up to 3 nm in high vacuum. Some photographs of the microstructure were obtained using a Hitachi SU3500 (Hitachi High-Technologies, Tokyo, Japan) scanning electron microscope [21].

Microstructure parameters were evaluated using a BX-51 research optical microscope with a U-CMAD3 digital camera (Olympus, Tokyo, Japan) and a SIAMS 800 image analyzer (SIAMS, Yekaterinburg, Russia).

The apparent density was determined in a factory certified laboratory, according to GOST 2409-95 «Refractories. Method for determination of apparent density, open, total and closed porosity, water absorption». The essence of this method lies in the fact that the dried sample is weighed, evacuated, and saturated with a liquid that moistens the sample but does not interact with it. The test sample was then weighed in a saturating liquid and in air. Based on the weighing carried out and the value of

the true density of the material, the apparent density, open and total porosity, and water absorption were calculated.

The determination of the microhardness of the samples was carried out with the indentation method using the Vickers method. A diamond pyramid was used as an indenter, and the pressure force was 500 N.

X-ray phase analysis of the powders and the obtained samples was carried out using an X´PertPRO X-ray diffractometer (Malvern Panalytical, Almelo, Netherlands, 2005) [22].

Designations of the studied samples are the following:
BT-30 – serial sample that does not contain nanoparticles;
B1 – sample with a content of 0.1 wt.% of TiO_2 nanoparticles;
B2 – sample with a content of 0.5 wt.% of TiO_2 nanoparticles;
B3 – sample with a content of 1.0 wt.% of TiO_2 nanoparticles;
B4 – sample with a content of 1.5 wt.% of TiO_2 nanoparticles;
B5 – sample with a content of 2.0 wt.% of TiO_2 nanoparticles.

3. Results and discussion

Beryllium and titanium oxides are thermodynamically stable over a wide temperature range. During sintering of ceramics in a reducing gas atmosphere, the TiO2 contained in the initial mixture is reduced according to the reaction:

$$TiO_2 \rightarrow Ti_nO_m + O_2.$$

The surface is rearranged when reduced TiO_2 single crystals are oxidized at moderate temperatures (200–390°C). Interstitial Ti atoms diffuse from the volume to the surface, where they react with gaseous oxygen and form new, added TiO_2 layers [23]. According to the response to heat treatment in oxygen, absorption bands in the visible region are attributed to Ti^{3+} and Ti^{2+} [24]. When such BeO + TiO_2 ceramics are sintered in a vacuum furnace with a graphite heater, under the influence of carbon at a high temperature, TiO_2 reduction proceeds according to the reaction:

$$TiO_2 + C = TiO + CO.$$

In this case, the presence of nano- and micropores, boundary segregations, a decrease in the surface energy at the boundaries of crystals, and the corresponding morphology and uniformity of their size distribution contribute to the thermal stability of the composite. The injection of vacancies into the crystal increases the free energy of the system and makes its growth thermodynamically unfavorable in a certain size range. Thus, an increase in the sintering temperature of such ceramics will promote a more efficient transformation of the TiO_2 crystal structure into a conductive rutile Ti_3O_5 form, and the formation of an electrically conductive phase; also, the ferromagnetic properties of nanoparticles will probably be accompanied by the absorption of electromagnetic energy [25]. By optimizing the structure, an optimal value of reflection losses can be achieved [26]. Changes in structural parameters due to the presence of nanoparticles can contribute to multiple re-reflection and energy absorptions [27]. Under the influence of heat treatment, anatase and brookite transform into rutile at temperatures of 400–1,000°C [28]. The most stable high-temperature form of these is rutile:

$$Brookite \xrightarrow{650^\circ C} Anatase \xrightarrow{915^\circ C} Rutile$$

The absorbing properties of (BeO + TiO_2)-ceramics are also due to the presence of non-stoichiometric Ti_3O_5 in their composition, the formation of which is facilitated by firing in a hydrogen atmosphere according to the reaction:

$$3TiO_2 + H_2 \rightarrow Ti_3O_5 + H_2O.$$

Thus, a quantitative change in the ratio of titanium-containing phases, as well as control of the degree of non-stoichiometry (reduction) of titanium oxides, will make it possible to develop absorbent titanate materials of various types.

Taking into account that the sintering temperature of ceramics is 1,520–1,530°C, the study of the

Table 3. Change in apparent density from the sintering temperature of (BeO + TiO_2)-ceramics with the addition of TiO_2 nanoparticles within 0.1–2.0 wt.%

Batch No.	Sintering temperature, °C	Composition of the ceramics	Density, g/cm^3
BT-30	1,530	BeO + 30.0% $TiO_2^{\mu m}$	3.2
B1	1,520	BeO+ 29.9% $TiO_2^{\mu m}$ + 0.1% TiO_2^{nano}	3.11
		BeO+ 29.5% $TiO_2^{\mu m}$ + 0.5% TiO_2^{nano}	3.13
		BeO+ 29.0% $TiO_2^{\mu m}$ + 1.0% TiO_2^{nano}	3.15
		BeO+ 28.5% $TiO_2^{\mu m}$ + 1.5% TiO_2^{nano}	3.15
		BeO+ 28.0% $TiO_2^{\mu m}$ + 2.0% TiO_2^{nano}	3.16
B2	1,530	BeO+ 29.9% $TiO_2^{\mu m}$ + 0.1% TiO_2^{nano}	3.23
		BeO + 29.5% $TiO_2^{\mu m}$ + 0.5% TiO_2^{nano}	3.23
		BeO+ 29.0% $TiO_2^{\mu m}$ + 1.0% TiO_2^{nano}	3.23
		BeO+ 28.5% $TiO_2^{\mu m}$ + 1.5% TiO_2^{nano}	3.22
		BeO+ 28.0% $TiO_2^{\mu m}$ + 2.0% TiO_2^{nano}	3.23
B3	1,540	BeO+ 29.9% $TiO_2^{\mu m}$ + 0.1% TiO_2^{nano}	3.22
		BeO+ 29.5% $TiO_2^{\mu m}$ + 0.5% TiO_2^{nano}	3.23
		BeO+ 29.0% $TiO_2^{\mu m}$ + 1.0% TiO_2^{nano}	3.22
		BeO+ 28.5% $TiO_2^{\mu m}$ + 1.5% TiO_2^{nano}	3.22
		BeO+ 28.0% $TiO_2^{\mu m}$ + 2.0% TiO_2^{nano}	3.22
B4	1,550	BeO+ 29.9% $TiO_2^{\mu m}$ + 0.1% TiO_2^{nano}	3.22
		BeO+ 29.5% $TiO_2^{\mu m}$ + 0.5% TiO_2^{nano}	3.23
		BeO+ 29.0% $TiO_2^{\mu m}$ +1.0% TiO_2^{nano}	3.22
		BeO+ 28.5% $TiO_2^{\mu m}$ + 1.5% TiO_2^{nano}	3.23
		BeO+ 28.0% $TiO_2^{\mu m}$ + 2.0% TiO_2^{nano}	3.22

effect of addition of TiO_2 nanoparticles in the range of 0.1–2.0 wt.% on the technological properties of (BeO TiO_2)-ceramics was carried out, and the results are presented in Table 3.

As mentioned above, the optimal sintering temperature for ceramics is 1,520–1,530°C. Above this temperature, the sample loses its density and geometric parameters, and swells (Figure 4).

It was found that when the sintering temperature reaches 1,530°C, the maximum value of the apparent density is reached at 3.23 g/cm^3, which does not decrease with an increase in the sintering temperature up to 1,550°C (Table 3).

Sintering efficiency strongly depends on the concentration of TiO_2^{nano}. The following are two boundary case interactions of chemical elements in the studied ceramics: the nanoparticles are chemically inert with respect to the micron matrix, as in the case of the BeO + $TiO_2^{\mu m}$ + TiO_2^{nano} system; the nanoparticles interact with the micron matrix, as in the case of the $TiO_2^{\mu m}$ + TiO_2^{nano} system. It can be seen that, upon sintering ceramics with nanoparticles, the density of the samples at $T_s > 1{,}530$°C is

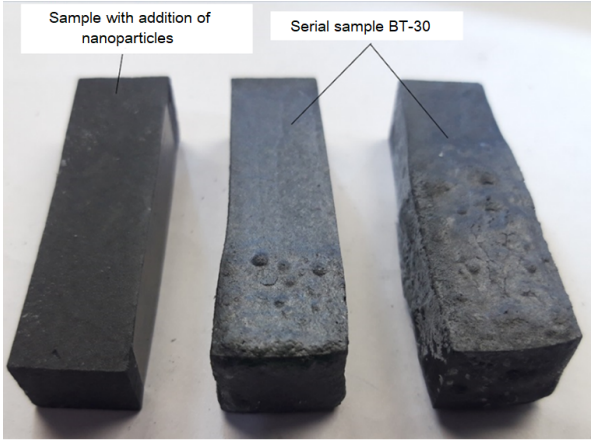


Fig. 4. Appearance of blanks sintered at 1,550°C, which are made, respectively, of ceramic to which TiO_2 nanoparticles (1.0%) have been added and serial ceramic BT-30 material

not lower than in the case of the initial sample. In the case of TiO_2 nanoparticles inert with respect to the BeO matrix, due to blocking of grain boundaries, the density of sintered samples does not increase with an increase in the sintering tempera-

ture. The results of studying the values of water absorption and porosity of such ceramics are presented in Table 4.

Table 4. Water absorption, and open, total, and closed porosities of BeO ceramics, depending on the content of TiO_2^{nano} (0.1%–2.0%)

Batch No.	Water absorption, %	Porosity, %		
		Open	Total	Closed
BT-30	0.03	0.10	7.076	6.977
B1	0.06	0.187	5.92	5.73
B2	0.05	0.165	5.329	5.164
B3	0.07	0.211	5.329	5.118
B4	0.06	0.186	5.031	4.845
B5	0.07	0.217	4.126	3.909

According to the results of studying the porosity of ceramics, it was found that, in comparison with a serial sample modified with nanoparticles in the amount of 0.1–2.0 wt.%, ceramics have a slightly increased water absorption, as a result of which they have a more pronounced open porosity, whereas the total and closed porosities have, on the contrary, lower values.

At the same time, on the best samples, despite the increased porosity, the apparent density reaches 3.33 g/cm^3. In terms of the combination of properties, the best results are shown by ceramics alloyed with nanodispersed titanium dioxide in the amount of 0.5 –1.5 wt.%.

The results of studying the microhardness of samples containing nanoparticles in comparison with a serial sample are shown in Figure 5.

A ceramic sample with an addition of 0.1 wt.% nanoparticles has a maximum value of microhardness of 9.6 GPa; with a nanoparticle content of 0.5–1.0 wt.%, the microhardness slightly decreases to 9.55 GPa; and with a further increase in nano-additives, the microhardness decreases to 9.5 GPa at 1.5 wt.% and 9.4 GPa at 2.0 wt.%. The microhardness of the sample without nano-additives is 9.33 GPa.

The observed increase in the microhardness of ceramics is associated with a change in microstructure under the influence of nanoparticles. The results of studying the microstructure of composite ceramics BT-30, manufactured using the same technology that is deployed for commercial production, showed that it is a mechanical mixture, as indicated in Figure 6.

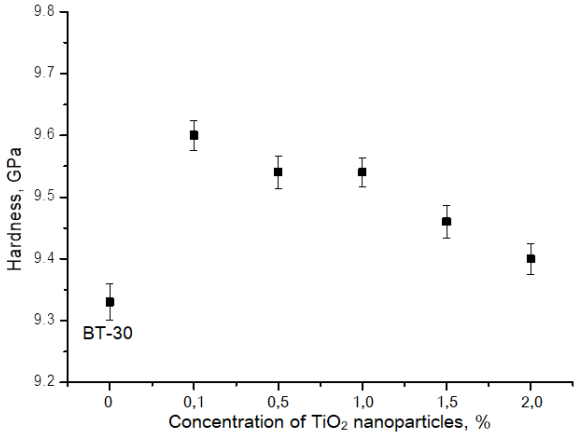


Fig. 5. Graph indicating the dependence of the change in the microhardness of samples on the content of nanoparticles (0.1%–2.0%)

Microstructural analysis of the sample mainly allows visualizing the distribution of elements and highlighting the phases. Thus, the white color represents the TiO_2 phase, and the dark color the BeO phase.

The results of measuring the particle sizes of BT-30 ceramics are shown in Figure 7. The total number of measured particles was 719 pcs. The smallest size of 0.5–1.0 μm has only 2 particles, the largest number of particles – 334 pcs., have a size of 1.0–5.0 μm, then from 5.0 to 10.0–199 particles, from 10.0–15.0 μm – 100 particles and then sizes of particles keeps decreasing. The largest particles have a size of 50 μm.

The evolution of the microstructure of ceramics after the addition of TiO_2 nanoparticles in the temperature range of 1,500–1,550°C is shown in Figure 8.

Figure 8 shows that at a sintering temperature of 1,500°C, in the microstructure of the ceramics and against the background of large, ~20–25 μm-sized fragments of TiO_2 grains, there is a large quantity (1,212 pcs) of small grains having a size of 1.0–5.0 μm. Figure 8 shows that at a sintering temperature of 1,500°C in the microstructure of the ceramics on the background of large, about 20–25 μm

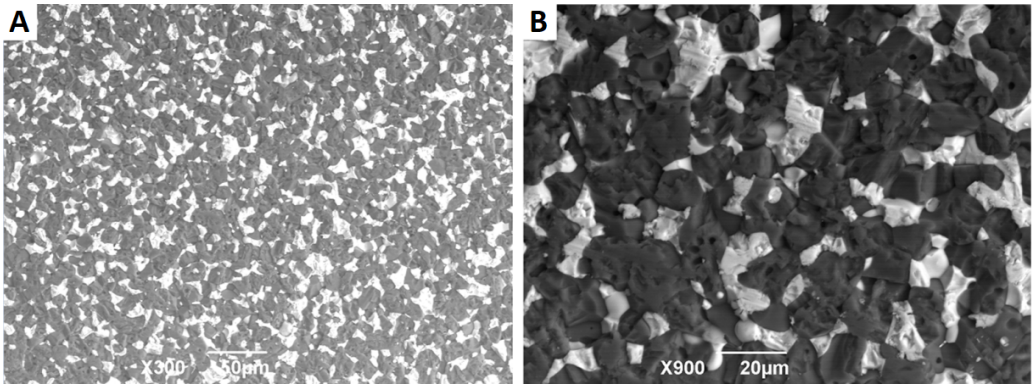


Fig. 6. Microstructure of BT-30 ceramic sample (BeO + 30 wt.% TiO_2) obtained from the initial BeO and TiO_2 powders having micron sizes: light – TiO_2; dark – BeO. **(A)** Magnification 300×; **(B)** Magnification 900×

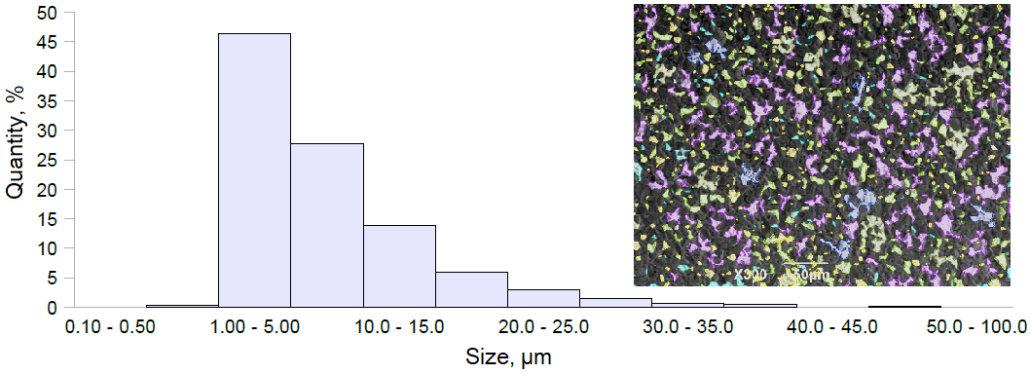


Fig. 7. Distribution of particle by size and quantity. Microstructure of BT-30 ceramics

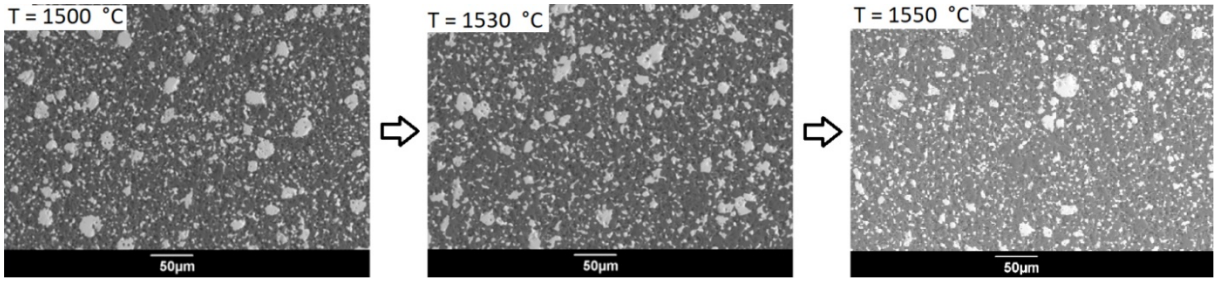


Fig. 8. Evolution of the microstructure of ceramics having a composition of BeO + 29.0% $TiO_2^{\mu m}$ + 1.0% TiO_2^{nano} under the influence of various temperatures

fragments of TiO_2 grains, there is a large quantity (1,212 pcs) and small grains ranging in size from 1.0 to 5.0 μm. As can be seen, the large TiO_2 elements have small ~0.5–1.0 μm globular pores. Apparently, given a particular micron particle size, the grouped TiO_2 nanoparticles, compared with the TiO_2 powder, give more shrinkage during sintering. It is also noticeable that the fragments of TiO_2 have an irregular shape, as if they penetrate into the intergranular spaces of BeO through better wettability and shrinkage of ceramics during sintering.

With increasing sintering temperature up to 1,530°C due to further compaction of the grain structure of large (20–25 μm) grains, the size of

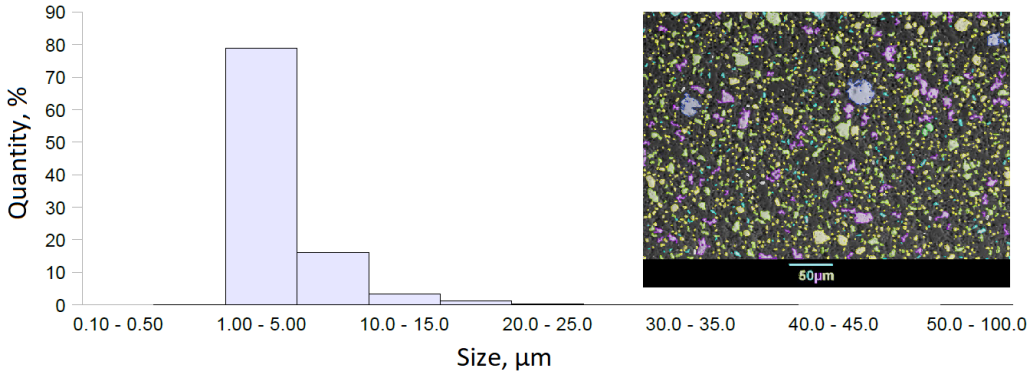


Fig. 9. Distribution of particle by size and quantity. Microstructure of BeO + 29.0% $TiO_2^{\mu m}$ + 1.0% TiO_2^{nano} ceramics. T= 1,550°C

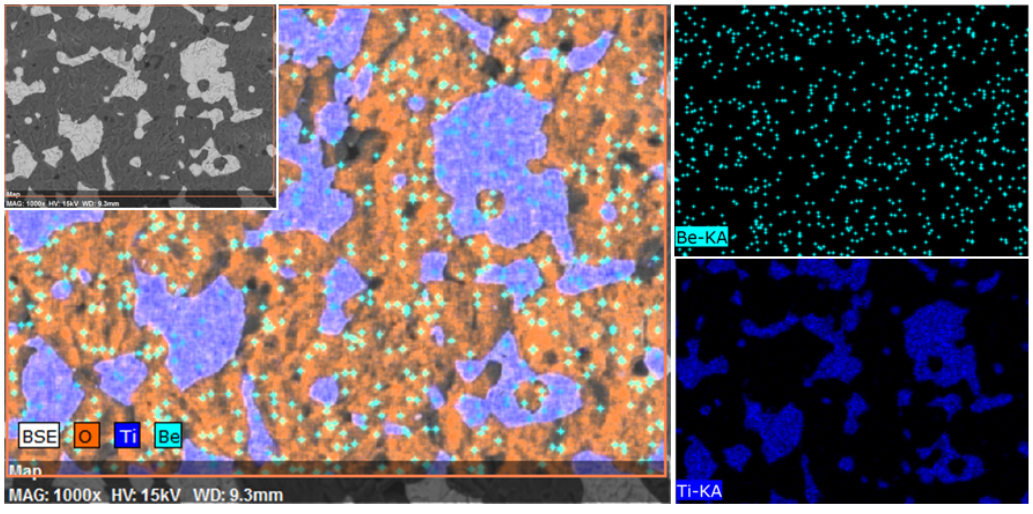


Fig. 10. Maps of phase distribution in ceramics of composition BeO + 28.5% $TiO_2^{\mu m}$ + 1.5% TiO_2^{nano}. T = 1,550°C

the TiO_2 particles does not reduce much, and globular pores increase in size to 1–2 µm and are partially self-healing, due to the interpenetration of the phases of TiO_2 and BeO.

The results of particle size measurements of sintered ceramics at T = 1,550°C are shown in Figure 9.

The total number of measured particles was 1,594 pcs. The smallest particle size of 0.5–1.0 µm characterizes only a single particle, the largest number of particles (1,257 particles) have a size of 1.0–5.0 µm, 257 particles have a size of 5.0–10.0 µm, 54 particles have a size of 10.0–15.0 µm, and from there onward, the particle size goes on diminishing. Further, the largest particles have the following sizes: 25.0–30.0 µm – 1 pc; 30.0–35.0 µm – 1 pc; and 50.0–100.0 µm – 1 pc.

Thus, with an increase in sintering temperature up to 1,550°C, the tendency to reduce the size of larger grains of TiO_2 remains, and the number of small grains significantly increases. Spherical pores increase in size and through them it is possible to observe the BeO phase, which is also a confirmation of the mechanism of self-healing of micropores due to penetration of the BeO phase in the voids of structural elements of TiO_2 (Figure 10) in the process of shrinkage of ceramics during sintering.

However, microscopic analysis of the phase boundary of BeO–TiO_2 at the nanoscale failed to

fix individual elements of the TiO_2 phase, as can be seen in Figure 11. The so-called diffusion barrier restraining crystal growth occurs at the initial stage of the sintering process. The identified improvements in the ceramics' structure and physical and mechanical properties are achieved due to the possibility of increasing the sintering temperature, which can in turn be attributed to the presence of the nanoparticles.

The phase electron microscopic analysis also indicates the interpenetration of TiO_2 in the intergrain spaces of BeO during sintering shrinkage of ceramics (Figure 11).

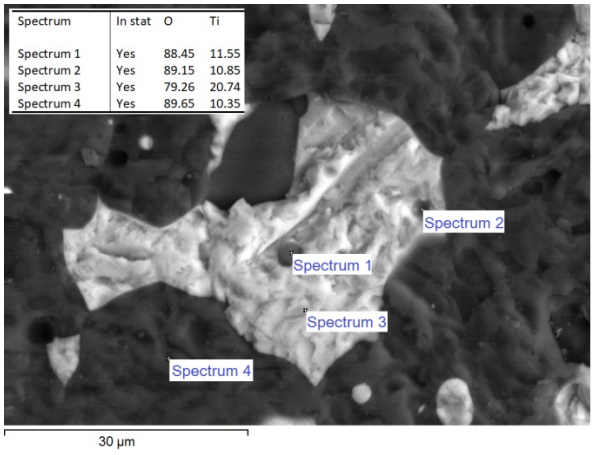


Fig. 11. Point energy dispersive X-ray spectroscopy (EDS) analysis of the grain structure of BeO + 28.5% $TiO_2^{\mu m}$ + 1.5% TiO_2^{nano} ceramics. T = 1,550°C

Since the Be is a relatively "light" chemical element, the technical capabilities of the electron probe do not allow its detection. The analysis is possible visually, using the color of the phase and the oxygen mass; for BeO – spectra 1, 2, and 4: it is 88.45–89.65 wt.%; and for TiO_2 – spectrum 3: it is ~79 wt.% (see inset in Figure 11).

Since the driving force of the sintering process is a decrease in the total surface energy, an increase in the volume fraction of grain boundaries and the density of defects arising from nanodispersed additives activates the sintering processes. From the maps of the distribution of chemical elements shown in Figure 10, it can be seen that the addition of TiO_2 nanoparticles leads to a higher density after sintering due to the interpenetration of TiO_2 and BeO phases, which is due to an increase in the diffusion mobility of atoms that in turn arises from an increase in the imperfection of the structure and the fraction of grain boundaries. The presence of nanoparticles promotes self-healing of micropores, which is apparently explained by the blocking of a certain fraction of the interfaces between the BeO particles by nanoparticles and the creation of a diffusion barrier.

The obtained diffraction patterns of the samples indicate the polycrystalline structure of the samples, as shown in Figure 12.

BT-30 – commercial sample, B1–B5 – samples sintered at a temperature of 1,550°C with various concentrations of TiO_2 nanoparticles (0.1–2.0 wt.%).

The main contribution, according to the phase analysis carried out in the structure of the ceramics, corresponds to the phases of titanium dioxide (rutile) and beryllium oxide. The structure also contains inclusions characteristic of the phases of tetragonal TiH_2 and orthorhombic Ti_3O_5 (Figure 13), the content of which vary depending on the concentration of nanoparticles. The deviation of the crystal lattice parameters is associated with deformation processes occurring because of the formation of ceramics, as well as the presence of impurity phases and solid solutions of substitution and interstitiality.

The main microwave radiation absorbing phase in the BT-30 material is the semiconductor nonstoichiometric compound Ti_3O_5, which is formed during the reduction of TiO_2 during the heat treatment of ceramics in a hydrogen atmosphere. Thus, an increase in the sintering temperature of ceramics due to the introduction of TiO_2 nanoparticles in the amount of 0.1–2.0 wt.% contributes to the creation of a reducing atmosphere and special conditions for a more efficient reduction of TiO_2 into the conductive compounds Ti_3O_5 and TiH_2.

In the future, the authors of the work plan to investigate the ability of synthesized ceramics to absorb and reflect electromagnetic radiation in the ultra-high frequency wavelength range.

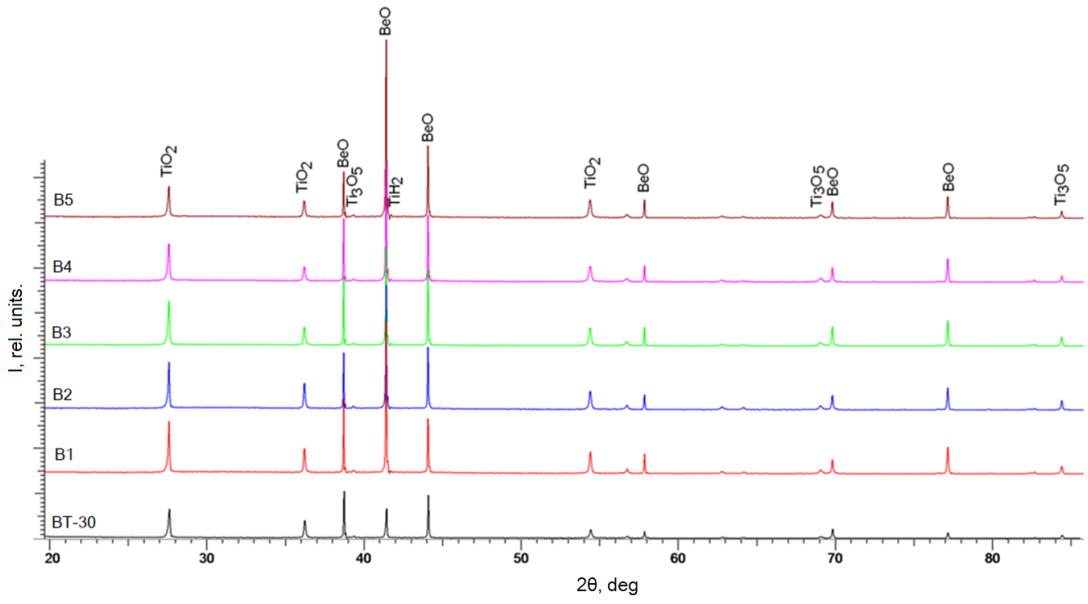


Fig. 12. X-ray diffraction patterns of the studied ceramics

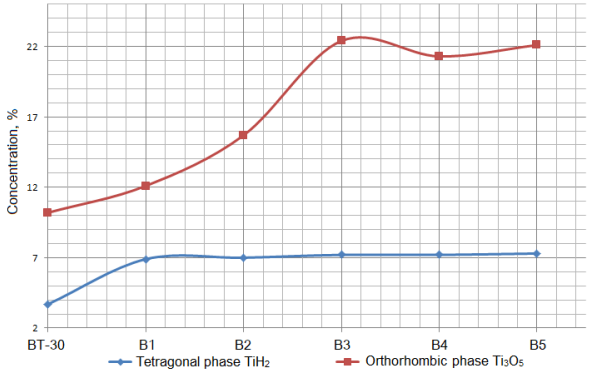


Fig. 13. The concentration of tetragonal and orthorhombic phases in the studied ceramics, depending on the number of introduced TiO_2 nanoparticles at the sintering temperature of T = 1,550°C

4. Conclusions

An increase in the volume fraction of grain boundaries and the density of defects arising from nanodispersed additives activates the sintering processes. The study of the effect of the firing temperature on the physico-mechanical properties of ceramics showed that the most effective amount of TiO_2 nanoparticles is within 0.1–1.5 wt.%. With the same composition, it is possible to increase the sintering temperature of the ceramic by 30°C.

As a result of measuring the particle sizes of synthesized ceramics, compared with the serial sample, it is found that there is a greater number of particles of the TiO_2 phase in the structure of experimental samples. There are more TiO_2 grains with the size of 1.0–5.0 μm (1,594 pcs) in comparison with the measurements of the serial sample (719 pcs).

The addition of TiO_2 nanoparticles leads to an increase in the density and microhardness of the sintered ceramics, due to the interpenetration of the TiO_2 and BeO phases, which is in turn attributable to an increase in the diffusion mobility of atoms arising from an increase in the imperfection of the structure and the fraction of grain boundaries.

The study of the effect of the firing temperature on the microstructure of ceramics with the addition of TiO_2 nanoparticles indicates the mechanism of self-healing of micropores by the penetration of the TiO_2 phase into the voids of the intergranular spaces of BeO in the process of ceramic shrinkage during sintering.

According to XRD data, an increase in the sintering temperature of ceramics containing nanoparticles of 0.1–2.0 wt.% TiO_2^{nano} up to 1,550°C promotes transformation of the crystalline structure of

TiO_2 into the more conductive Ti_3O_5, which has an orthorhombic structure and can be accompanied by absorption of electromagnetic radiation.

Funding

This research was funded by the Science Committee of the Ministry of Education and Science of the Republic of Kazakhstan (Grant No. AP09058686).

References

[1] Qing YC, Zhou WC, Luo F, Zhu DM. Titanium carbide (MXene) nanosheets as promising microwave absorbers. Ceram Int. 2016;42:16412–6.

[2] Lu G, Wancheng Z, Fa L, Dongmei Z, Jie W. Dielectric and microwave absorption properties of KNN/Al_2O_3 composite ceramics. Ceram Int. 2017;43(15): 12731–5.

[3] Drokin NA, Kiyko VS, Pavlov AV, Malkin AI. Electrophysical properties of BT-30 ceramics. New Refract. 2020;6:56–63 [in Russian].

[4] Bukharin Ye N, Ilyina Ye N. Volumetric absorbers of microwave energy in the designs of modern vacuum microwave devices and measuring devices. M Radiotekhnika 2014;15(11):57–64 [in Russian].

[5] Mo S, Ching W. Electronic and optical properties of three phases of titanium dioxide: Rutile anatase brookite. Phy Rev B 1995;51(19):13023–32.

[6] Moravis EV, Olivera RGM, Castro AJN. Dielectric study in the microwave range for ceramic composites based on Sr_2CoNbO_6 and TiO_2 mixtures. J Electron Mater. 2017;46(8):5193–200.

[7] Oliveira RGM, Morais JEV, Freitas DB. The effects of TiO_2 addition on the dielectric and microwave properties in the ceramic matrix $BiVO_4$. In: International Conference on Intelligent Circuits and Systems (ICICS), Phagwara, India, 19–20 April 2018; 2018. pp. 461–4.

[8] Lyapin LV, Pavlova MA, Semenyuk SS. Energy absorbers for microwave devices. Compon Technol. 2009; 11:126–28 [in Russian].

[9] Kiiko VS, Pavlov AV. Composite (BeO+TiO_2)-ceramic for electronic engineering and other fields of technology. Refract Ind Ceram. 2018;57(6):423–6.

[10] Polyanskaya T.I., Panitskov V.I., Zharikhin S.V. Designing a retarding system for continuous Ku band TWTs with an operating frequency band of at least 16.5% and a gain of at least 30 dB. Microwave Electron Microelectron. 2019;1(1):379–86 [in Russian].

[11] Kolomiytseva NM, Bakunin GV, Polyanskaya TI, Panitskov VI, Filin Yu Y. Design of the slowing down system "looping waveguide" for the development of industrial basic technology for the manufacture of TWT in the W band. Microwave Electron Microelectron. 2018;1:148–54 [in Russian].

[12] Kiiko VS, Makurin Yu N, Ivanovskiy AL. Ceramics based on beryllium oxide: preparation, physicochemical properties and application. Yekaterinburg: UB RAS, 2006: 440 [in Russian].

[13] Kiiko VS. The influence of titanium dioxide additives on the physicochemical and luminescent properties of beryllium ceramics. Inorgan Mater. 1994;30(5):688–93 [in Russian].

[14] Kiiko VS, Gorbunova MA, Makurin Yu N. Microstructure and electrical conductivity of the composite (BeO + TiO_2)-ceramics. New Refract. 2007;11:68–74 [in Russian].

[15] Kiiko VS, Shabunin SN, Makurin Yu N. Obtaining, physicochemical properties and transmission of microwave radiation by ceramics based on BeO. Refract Tech Ceram. 2004; 10: 8–17 [in Russian].

[16] Kiiko VS, Pavlov AV. Ceramic for electronic engineering and other fields of technology. Refract Ind Ceram. 2018;58(6):687–92.

[17] Kiiko VS, Pavlov AV, Bykov VA. Production and thermophysical properties of BeO ceramics with the addition of nanocrystalline titanium dioxide. Refract Ind Ceram. 2019;59(6):616–22.

[18] Lepeshev AA, Pavlov AV, Drokin NA, Malkin AI, Kiiko VS, Knyazev NS. Features of the preparation and study of electrophysical characteristics (BeO+TiO_2)-ceramics by impedance spectroscopy. Refract Ind Ceram. 2019;60(3):309–17.

[19] Malkin A, Korotkov A, Knyazev N, Kijko V, Pavlov A. Approbation of the measurement method to determining the permittivity of micro- and nanopowders of titanium dioxide. In: International multi-conference on engineering, computer and information sciences, Novosibirsk, Russia, 21–27 October 2019; 2019, pp. 217–20.

[20] Khaibullin RI, Tigirov LR, Ibragimov Sh Z. Ferromagnetism and two magnetic phases in rutile (TiO2) implanted with cobalt ions. Kazan. 2007;149(3):31–41 [in Russian].

[21] Rakhadilov B, Kenesbekov A, Skakov M, Miniyzov A. Hydrogen and deuterium storage in tungsten when irradiation with Plasma beam. MetalConf, 2018; 27: pp. 1216-1221.

[22] Rahadilov BK, Zhurerova LG, Sagdoldina ZB, Kenesbekov AB, Bayatanova LB. Morphological Changes in the Dislocation Structure of Structural Steel 20GL after Electrolytic-Plasma Hardening of the Surface. Journal of Surface Investigation, 2021;15(2):408-413.

[23] Li M, Hebenstreit W, Diebold U. Morphology change of oxygen-restructured TiO2 (110) surfaces by UHV annealing: formation of a low-temperature (1×2) structure. Phys Rev B. 2000;61(7):4926–33.

[24] Sekiya T, Kamei S, Kurita S. Luminescence of anatase TiO_2 single crystals annealed in oxygen atmosphere. J Lumin. 2000;87–9:1140–42.

[25] Tikhov VA, Yatsyshen VV. Features of the scattering of a high-frequency electromagnetic field by a nanoscale ferromagnetic sphere. VolSU Bull. 2021;10(4):116–20 [in Russian].

[26] Lia Y, Chen Ch, Pan X, Ni Y, Zhang S, Huang J, et al. Multiband micro-wave absorption films based on defective multiwalled carbon nanotubes added carbonyl-

iron/acrylicresin. *Physica B*. 2009;404:1343–6.

[27] Rodionov V.V. Mechanisms of interaction of microwave radiation with nanostructured carbon-containing materials: CSc thesis FGBOU VO. Southwest State University, Kursk. 2015:169 [in Russian].

[28] Kandiel TA, Robben L, Alkaimad A, Bahnemann D. Brookite versus anatase TiO_2 photocatalysts: phase transformations and photocatalytic activities. Photochem Photobiol Sci. 2013;12(4):602–9.

Received 2021-12-07
Accepted 2022-04-02